Journal of Luminescence 132 (2012) 784–788

Contents lists available at SciVerse ScienceDirect

Journal of Luminescence

journal homepage: www.elsevier.com/locate/jlumin

Mid-infrared emissions from Ho^{3+} in Ga_2S_3-GeS_2-Sb_2S_3 glass

Manabu Ichikawa, Yo-ichi Ishikawa, Takashi Wakasugi, Kohei Kadono *

Graduate School of Chemistry and Materials Technology, Kyoto Institute of Technology, Matsugasaki, Sakyo-ku, Kyoto 606-8585, Japan

ARTICLE INFO

Article history:
Received 2 August 2011
Received in revised form
25 October 2011
Accepted 4 November 2011
Available online 10 November 2011

Keywords:
Sulfide Glass
Ho^{3+}
Mid-infrared Emission
Population Analysis
Low-Phonon Energy
Rare-Earth

ABSTRACT

Emission properties were investigated in the infrared region for Ga_2S_3-GeS_2-Sb_2S_3 glasses doped with Ho^{3+}. We performed Judd–Ofelt analysis and lifetime measurements of the $^5I_4$, $^5I_5$, and $^5I_6$ levels, which are the initial levels of the mid-infrared emissions between 3 to 5 μm of Ho^{3+}. The quantum efficiencies reached approximately 18%, 64%, and ~100% for the $^5I_4$, $^5I_5$, and $^5I_6$, respectively. Population analyses were carried out from the relative intensities of the emissions in the near-infrared region. We investigated the dependences on the Ho^{3+} ion concentration of the population ratio of the initial levels to the final levels, [initial]/[final], of the mid-infrared emissions. The population ratio of $[^5I_5]/[^5I_6]$ decreased with increase of the Ho^{3+} concentration while those of $[^5I_4]/[^5I_5]$ and $[^5I_6]/[^5I_7]$ increased. Particularly, the former, $[^5I_4]/[^5I_5]$, rapidly increased because of the strong concentration quenching of the $^5I_5$ level through cross relaxation. It was found that the population inversion for the 4.8 μm emission due to the transition, $^5I_4 \rightarrow {}^5I_5$, was achieved at high Ho^{3+} concentration in the present experiments.

1. Introduction

Laser oscillation operating in the mid-infrared region at room temperature provides potential applications to infrared in situ spectroscopy, such as chemical sensing and gas monitoring [1–3]. Recently, Moizan et al. have reported 4.6 μm emission due to the transition, $^4I_{9/2} \rightarrow {}^4I_{11/2}$, of Er^{3+} embedded in Ge-Ga-Sb-S based glass and fiber [4,5]. We also investigated the dependence of the emission properties of this transition on the glass composition and the concentration of Er^{3+} using a stoichiometric Ga_2S_3-GeS_2-Sb_2S_3 host glass [6,7]. The advantage of this transition for the mid-infrared emission is that the initial level, $^4I_{9/2}$, can be directly excited by an easily available laser diode having a wavelength shorter than 1 μm. It has been found, however, that the concentration quenching through energy transfers depopulates the initial level more rapidly than the final level ($^4I_{11/2}$). This makes the population inversion more difficult in addition to that the radiative lifetime of the initial level is shorter than that of the final level. Therefore, we have investigated other rare-earth ions, which can be used as an active ion for mid-infrared emissions. Holmium ion has received attention because it has several emissions in the infrared region [8–16]. Among them, 2.0 μm emission due to the transition, $^5I_7 \rightarrow {}^5I_8$, has been widely investigated [12–16]. However, there are a few reports on the transitions, $^5I_5 \rightarrow {}^5I_6$ and $^5I_4 \rightarrow {}^5I_5$, which emit fluorescence around 3.9 μm and 4.8 μm [8–11,14]. Since the energy gaps between the initial levels and the just lower levels are very small (less than 2600 cm^{-1}) for these transitions, it is necessary to use extremely low phonon energy matrices, such as chalcogenides and non-fluoride-halides, as a host material in order to obtain high efficiency of the emission [3,8,17]. Purpose of this work is to investigate the emission characteristics of the $^5I_6$, $^5I_5$, and $^5I_4$ levels of Ho^{3+} in the Ga_2S_3-GeS_2-Sb_2S_3 host glass, particularly, paying attention to the dependences on the Ho^{3+} concentration and energy transfers between ions. We found that the population of the $^5I_4$ level was hardly affected by the Ho^{3+} concentration within the range of the present work whereas the $^5I_5$ level was rapidly depopulated through a cross relaxation. This is advantageous to obtain population inversion for the 4.8 μm emission due to the $^5I_4 \rightarrow {}^5I_5$ transition.

2. Experimental procedures

The $20GaS_{3/2} \cdot 50GeS_2 \cdot 30SbS_{3/2} \cdot xHoS_{3/2}$ glasses (x=0.3, 1, 3, and 5) were prepared in evacuated silica tubes by a conventional melting-cooling method for chalcogenide glasses. The starting reagents were Ga (7N), Ge (4N), Sb (5Nup), Ho (3N), and S (6N). Sulfur was distilled to remove the impurity water before use. More details for glass preparation were described elsewhere [18]. The glass transition temperature and density of the host glass, $20GaS_{3/2} \cdot 50GeS_2 \cdot 30SbS_{3/2}$, were 321 °C and 3.26 g cm^{-3}, respectively. Refractive indices were 2.40, 2.31, and 2.28 at 633, 980, and 1544 nm, which were measured using a prism coupler (model 2010, Metricon).

* Corresponding author. Tel./fax: +81 75 724 7565.
E-mail address: kadono@kit.ac.jp (K. Kadono).

0022-2313/$ - see front matter © 2011 Elsevier B.V. All rights reserved.
doi:10.1016/j.jlumin.2011.11.007

Absorption spectra were measured using a spectrophotometer (UV-3100, Shimadzu) in the wavelength region from 400 to 2500 nm. Emission spectra were measured in the range from 1 to 5.5 μm. Emissions from the sides of the samples excited using a Ti:sapphire laser were detected by an InSb detector (EG&G) cooled at liquid N_2 temperature. The optical setup was calibrated using a standard halogen lamp (QTH source, Newport) in the near-infrared region (from 1 to 2.4 μm) in order to remove the wavelength dependence of efficiency.

The decay curves of 1255 nm and 1660 nm emissions due to the $^5I_4 \rightarrow {}^5I_7$ and $^5I_5 \rightarrow {}^5I_7$ transitions were measured by the direct excitation of the initial levels, and the lifetimes were obtained with the $1/e$ holding time. The lifetime of the $^5I_6$ level was evaluated by a single exponential curve-fitting for the decay curve of the 1180 nm due to the transition, $^5I_6 \rightarrow {}^5I_8$, by the excitation at $^5I_5$ in the range of sufficiently large time. The data of decay curves were stored to a digital oscilloscope (waveRunner 64xi, or 9350A, LeCroy). Pulsed laser beam was obtained by chopping the c.w. laser beam using a mechanical chopper.

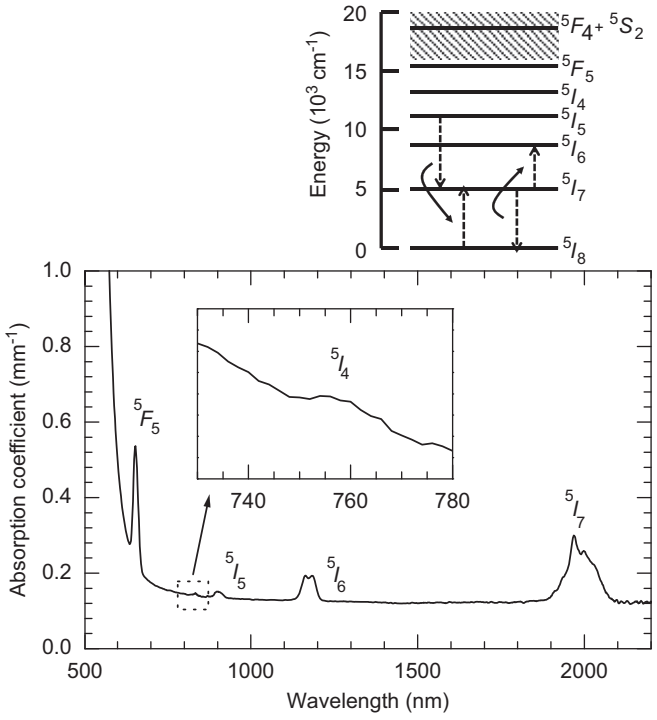

Fig. 1. Absorption spectrum of $20GaS_{3/2} \cdot 50GeS_2 \cdot 30SbS_{3/2} \cdot 3HoS_{3/2}$ glass and energy diagram of 4f orbital of Ho^{3+} showing energy transfers expected to occur at high Ho^{3+} concentration (see text). Hatched area shows that absorption bands to the levels in this area are not observed due to absorption of Ga_2S_3-GeS_2-Sb_2S_3 host glass.

3. Results and discussion

3.1. Judd–Ofelt analysis and mid-infrared emissions

Fig. 1 shows an absorption spectrum of $20GaS_{3/2} \cdot 50GeS_2 \cdot 30SbS_{3/2} \cdot 3HoS_{3/2}$ glass and energy diagrams of Ho^{3+}. Judd–Ofelt analyses were performed with the four observed absorption bands, $^5I_8 \rightarrow {}^5I_7$, $^5I_6$, $^5I_5$, and $^5F_5$, where the matrix elements calculated by Carnall et al. and Weber et al. were used [19–22]. The refractive indices used in the analysis were evaluated by interpolation with Cauchy equation and the indices measured at the three wavelengths (633 nm, 980 nm, and 1.54 μm). Since the $^5I_8 \rightarrow {}^5I_7$ transition has a large contribution from the magnetic dipole transition, we included the value of the magnetic dipole line strength [23,24]. Table 1 shows the results of the Judd–Ofelt analysis in which the estimated omega parameters were $\Omega_2 = 1.91 \times 10^{-19}$ cm^2, $\Omega_4 = 5.94 \times 10^{-20}$ cm^2, $\Omega_6 = 1.02 \times 10^{-20}$ cm^2. The lifetimes listed in the table were measured for the glass containing 0.3 mol% $HoS_{3/2}$. Assuming that the energy transfers between Ho^{3+} ions are ignored for this concentration, nonradiative relaxation rates were determined as the difference between the total radiative transition rates and the measured transition rates. The quantum efficiencies of the $^5I_4$, $^5I_5$, and $^5I_6$ levels are 18, 64, and ~100%; it is noteworthy that in spite of the small energy gaps between $^5I_4$ and $^5I_5$ (2100 cm^{-1}), and $^5I_5$ and $^5I_6$ (2600 cm^{-1}), the quantum efficiencies are large. Furthermore, it is noticeable that the branching ratios of the $^5I_4 \rightarrow {}^5I_5$ and $^5I_5 \rightarrow {}^5I_6$ transitions are more than 10%, compared with the small branching ratio (about 1%) of the 4.5 μm emission due to the $^4I_{9/2} \rightarrow {}^4I_{11/2}$ transition of Er^{3+}. Particularly, the $^5I_4$ level has not received much attention so far probably because of the weak absorption to this level and a small total radiative transition rate. Focused on the radiative transition rate for the $^5I_4 \rightarrow {}^5I_5$ transition, however, it is three times larger than that of the $^4I_{9/2} \rightarrow {}^4I_{11/2}$ transition of Er^{3+} (~10 s^{-1}) [4,6].

Table 1
Transition properties of the excited 4f levels of Ho^{3+} for $20GaS_{3/2} \cdot 50GeS_2 \cdot 30SbS_{3/2} \cdot 3HoS_{3/2}$ glass. The lifetimes were measured for the glass containing 0.3 mol% $HoS_{3/2}$ with the same glass composition.

Transition	Energy difference (10^3 cm^{-1})	$A(J \rightarrow J')$ (s^{-1})	$A(J)$ (s^{-1})	Branching ratio (%)	Lifetime τ (ms)	Emission relaxation rate (s^{-1})	Nonradiative relaxation rate (s^{-1})	Quantum efficiency (%)
$^5I_7 \rightarrow {}^5I_8$	5.08	304	304	100				
$^5I_6 \rightarrow {}^5I_8$	8.59	521	634	82	1.80	555	0	100
$^5I_7$	3.51	113		18				
$^5I_5 \rightarrow {}^5I_8$	11.14	198	459	43	1.39	718	259	64
$^5I_7$	6.07	210		46				
$^5I_6$	2.55	52		11				
$^5I_4 \rightarrow {}^5I_8$	13.23	22	248	8.8	0.740	1.35×10^3	1.10×10^3	18
$^5I_7$	8.15	105		42				
$^5I_6$	4.64	92		37				
$^5I_5$	2.09	29		12				
$^5F_5 \rightarrow {}^5I_8$	15.29	1.16×10^4	1.47×10^4	79				
$^5I_7$	10.21	2.67×10^3		18				
$^5I_6$	6.70	373		2.5				
$^5I_5$	4.16	28		0.19				
$^5I_4$	2.06	0.28		0.0019				